Author for correspondence:
Lucas K. Zoet, E-mail: lzoet@wisc.edu

Transient evolution of basal drag during glacier slip

Lucas K. Zoet[1] [ID], Neal R. Iverson[2], Lauren Andrews[3] and Christian Helanow[4]

[1]Department of Geoscience, University of Wisconsin- Madison, Madison, WI 53704, USA; [2]Department of Geological and Atmospheric Sciences, Iowa State University, Ames, IA 50011, USA; [3]Global Modeling and Assimilation Office, NASA Goddard Space Flight Center, Greenbelt, MD 20771, USA and [4]Department of Mathematics, Stockholm University, Stockholm, Sweden

Abstract

Glacier slip is usually described using steady-state sliding laws that relate drag, slip velocity and effective pressure, but where subglacial conditions vary rapidly transient effects may influence slip dynamics. Here we use results from a set of laboratory experiments to examine the transient response of glacier slip over a hard bed to velocity perturbations. The drag and cavity evolution from lab experiments are used to parameterize a rate-and-state drag model that is applied to observations of surface velocity and ice-bed separation from the Greenland ice sheet. The drag model successfully predicts observed lags between changes in ice-bed separation and sliding speed. These lags result from the time (or displacement) required for cavities to evolve from one steady-state condition to another. In comparing drag estimates resulting from applying rate-and-state and steady-state slip laws to transient data, we find the peaks in drag are out of phase. This suggests that in locations where subglacial conditions vary on timescales shorter than those needed for cavity adjustment transient slip processes control basal drag.

1. Introduction

Glacier slip velocity over both hard and soft beds is sensitively dependent on subglacial water pressure (Bindschadler, 1983; Iken and Bindschadler, 1986; Hooke and others, 1997; Zoet and Iverson, 2020) and the transients imposed by water pressure fluctuations (Harper and others, 2002, 2007; Bartholomaus and others, 2008; Andrews and others, 2014). In locations where surface water can penetrate to the glacier bed, subglacial water pressure may vary dramatically over timescales of hours to minutes (Iken, 1972; Cowton and others, 2013; Andrews and others, 2014; Covington and others, 2020), affecting the ice-bed coupling. In circumstances where subglacial water pressure is changing, glacier slip may be in a continuous state of adjustment in which steady-state conditions are never fully attained (Tsai and others, 2021). This transient condition is problematic for describing glacier slip, as most existing slip models are formulated only for steady-state conditions. Steady-state models are appropriate if the processes that regulate slip dynamics (e.g. cavity evolution) vary much more rapidly than subglacial conditions (e.g. water pressure). This is commonly not true, however, as indicated by observations of subglacial water pressure and slip velocity (e.g. Harper and others, 2007; Bartholomaus and others, 2008; Andrews and others, 2014), which motivates the question: how important are these transient effects in slip dynamics?

In numerous instances, subglacial water pressure and glacier flow velocity have been measured coeval and have been shown to relate to one another (Kamb and others, 1985; Iken and Bindschadler, 1986; Fischer and Clarke, 1997; Harper and others, 2002, 2007). In one example from the Greenland ice sheet (GIS), Andrews and others (2014) placed water pressure transducers down moulins and boreholes to document changes in subglacial water pressure stemming from diurnal patterns in surface meltwater production. In their study location, it was hypothesized that the glacier was slipping over a hard bed and that in some locations cavity development was widespread, whereas near the moulins well-developed channels had formed (Andrews and others, 2014). Their observations show a close link between flow velocity and moulin water pressure, but ice-bed separation related to subglacial cavity size lagged both increases in water pressure and ice motion.

Subglacial water flow affects drag on hard beds through its regulation of subglacial effective pressure, *N,* (overburden pressure minus water pressure). Hydrologic configurations affect N differently: an efficient system of channels (R channels) commonly supports high N whereas an inefficient system of linked cavities commonly supports low N (e.g. Flowers, 2015). For channels to form and remain open requires an abundant supply of meltwater, commonly from the glacier surface (e.g. Hewitt, 2011; Werder and others, 2013; Hoffman and Price, 2014), whereas linked cavities remain open primarily through sliding (Lliboutry, 1968, 1979; Walder, 1986). The ability of linked cavities to exist independent from surface meltwater input allows them to persist throughout winter months and likely span much of the glacier base. Cavity geometry depends on the ice slip velocity and the water pressure (Walder, 1986; Kamb, 1987) and directly affects basal drag. Cavity growth causes drag to be supplied by progressively smaller parts of the bed, with adverse bed slopes in areas of ice-bed contact dictating the balance of forces (Iken, 1981; Helanow and others, 2020, 2021). Therefore, the

state of the ice-bed contact regulates glacier flow velocity but is acutely sensitive to changes in subglacial water pressure.

A complicating factor often neglected in force balance estimates is the time-dependent drag response to a change in velocity (or water pressure) stemming from the finite time (or displacement) required for cavity geometry to readjust to the new conditions. If cavity geometry needs to adjust only a small amount when transitioning from one steady-state condition to another, the transient associated with geometry readjustment (and drag) may be short-lived and unimportant. In contrast, if the prevailing cavity geometry is far from the new steady state, the transient may require an extended period of time (or displacement) to reach the new steady state, and transient drag evolution may largely control slip.

Slip laws relate drag, velocity and effective pressure and are usually formulated in terms of steady-state conditions. For any slip law, the transient response in drag to a finite velocity change could deviate from the steady-state relationship (Fig. 1). The glacier must then overcome the transient drag to reach the new steady state. This path effect is important irrespective of the form of the steady-state slip law. This scenario becomes more complicated when, rather than simply moving from one velocity-drag, steady-state condition to another, conditions continually vary, as is commonly observed beneath glaciers (e.g. Andrews and others, 2014).

Herein, we study with laboratory experiments slip of temperate ice over a hard bed at various slip velocities and measure drag and cavity evolution in response to near-instantaneous velocity steps. This information is used to constrain a transient slip evolution model based on the framework provided by rate-and-state friction (RSF). The laboratory-derived slip model is then applied to a glacier of the GIS where continuously recorded surface velocities are used to drive the RSF model. Through this application, the transiently evolving basal drag can be estimated. We compare the timing of a field proxy for ice-bed separation with the timing of cavity evolution predicted by the RSF model. We then interpret the physical processes of glacier slip in terms of the time lags among drag, cavity geometry and slip velocity.

2. Methods

2.1 Experiments

A large-diameter, ring-shear device (Iverson and Petersen, 2011) (Fig. S3) is used to slide a ring of temperate ice over a rigid sinusoidal bed (Fig. 2). The device is housed in a walk-in freezer, while the chamber that contains the ice ring is submerged in an ethylene glycol/water mixture. This fluid is connected to an external circulator that regulates the fluid temperature. This system allows the ice to be held at the pressure-melting temperature (PMT) for months at a time with minimal melt, so that large-displacement experiments can be conducted. Twelve rigid, sinusoidal bed pieces (centerline wavelength is 183 mm and amplitude is 15.3 mm) fit together to constitute the bed at the base of the ice chamber (Fig. 2). The bed is made of Delrin, which is a polymer with a low friction coefficient and low thermal conductivity. The low thermal conductivity minimizes regelation (Zoet and Iverson, 2015). During experiments at the PMT, a thin film of liquid water at the ice-bed interface minimizes frictional drag, so that nearly all measured drag results from ice deformation past bed obstacles.

An ice ring is constructed atop the bed by sequentially flooding ~2 cm thick layers of crushed deionized ice with chilled deionized water until the ring is ~20 cm thick. Resultant randomly oriented ice crystals develop a c-axis fabric during flow past bumps that is similar to those of glacier basal ice (see Zoet
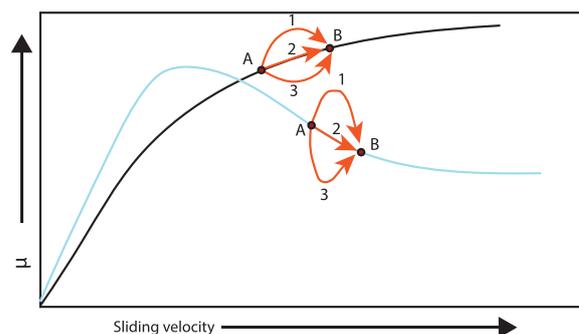

Fig. 1. Steady-state slip laws. The black line is a rate-strengthening slip law, whereas the blue line is a double-valued slip law with both rate-strengthening and rate-weakening components. The transition from A to B in response to an increase in velocity could have various paths. Path 1 represents a transient strengthening of the system, whereas path 3 represents a transient weakening of the system. Path 2 follows the steady-state slip law. If the velocity-drag path follows path 2, there is no need to account for transient effects. If the path follows 1 or 3, deviating substantially from the steady-state path, then transient effects need to be accounted for if the timescale of interest is sufficiently short and the deviation is sufficiently large.
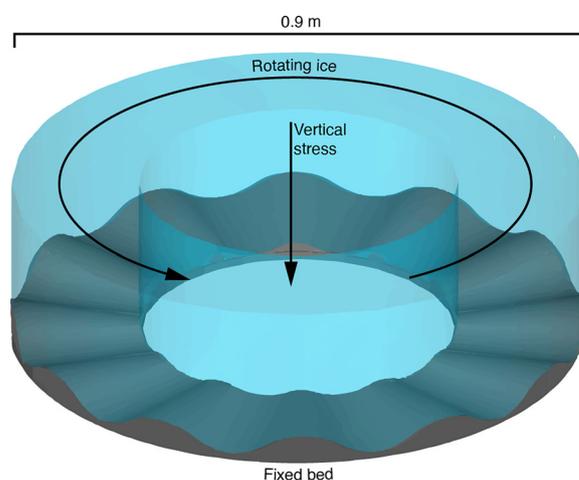
Fig. 2. Schematic of the bed and ice ring used in these experiments. A ring of ice, 0.9 m in outer diameter, is pressed against a sinusoidal bed made of Delrin. The ice ring is gripped at its upper surface by a platen and dragged over the bed, which is fixed rotationally but moves up or down as the volume of the ice chamber that holds the ice ring changes due to changes in cavity size. The bed is designed so that adverse slopes of bumps do not vary radially.

and Iverson, 2015). Once the ice ring is constructed, the toothed upper platen is frozen into the upper surface of the ice ring. Total stress normal to the upper platen is regulated by a vertical hydraulic ram that can raise or lower the ice chamber to accommodate cavity growth or decay and melting during experiments. Meltwater can fill cavities, but excess water is drained through a series of 24 drainage ports at the inner and outer perimeter of the ice chamber. Water pressure, measured by four strain gauge water pressure transducers, is kept very near atmospheric, so N equals the vertical stress applied by the ram. A displacement transducer (LVDT) that is mounted at the base of the ice chamber measures its vertical displacement in response to cavity volume change and melting (Fig. S3; see supporting text S1 for a more detailed explanation of cavity volume estimates). Ice melts along the walls, top and base of the ice ring. Prior to the initiation of slip, the vertical contraction rate from melting is measured and subtracted from the vertical displacement record for the remainder of the experiment, allowing the residual vertical displacement to mainly be attributed to cavity expansion or contraction. More details on the device and experiments can be found in Zoet and Iverson (2015) and supporting text S1.
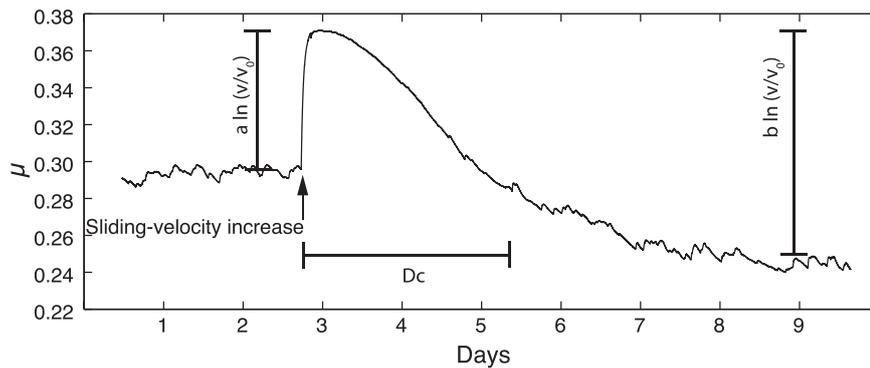
Fig. 3. Experimental drag. Time series of the drag ($\mu = \tau/N$) from a near-instantaneous increase in sliding velocity (indicated by arrow). The drag takes ~6 d to return to a steady-state value. The a parameter can be estimated from the time series to describe the magnitude of the sudden increase in drag (i.e. the direct effect), and the b parameter describes the magnitude of the subsequent decrease in drag to a steady value. D_c is the critical slip distance implied from the indicated duration and the slip velocity, 29 m a^{-1}. This velocity step is from 14.5 to 29 m a^{-1}. The difference a-b relates steady-state friction values at different velocities.

Once the ice ring is constructed and the ice has reached the PMT, motion is initiated by rotating the upper platen, which forces slip of the ice over the bed. A steady velocity is set, and the drive system forces the upper platen to rotate at that velocity while a sensor measures the torque required to rotate the platen, from which area-averaged drag (i.e. shear stress, τ) on the bed is calculated. The friction coefficient, μ, is estimated by normalizing the recorded drag, τ, by the measured effective stress, N. Vertical displacement measured by the LVDT allows continuous determination of cavity volume. When velocity is stepped, it increases essentially instantaneously. After a steady drag is reached, sometimes taking as long as 14 d, the velocity is again stepped (Fig. 3). In this study velocity was stepped to 14.5, 29, 58, 116 and 290 m a^{-1}, and effective pressure was held constant at 500 kPa (within 2%). The LVDT record provides a volume-integrated measurement of the cavity size but no information about cavity shape (see supporting text S1 for more details). After an experiment is over, the ice ring is extracted from the ice chamber, and the geometry of the ice sole (Fig. 4) is precisely measured using a custom-made jig. This process provides a measurement of cavity geometry at one steady-state sliding velocity (the final velocity, 290 m a^{-1}).

2.2 Observations from the Greenland ice sheet

We compare results from these experiments with observations of basal water pressures, ice surface velocity and ice-bed separation made in the Pâkitsoq region (69°27′N, 49°53′W) of the western GIS during the 2011 and 2012 summer melt seasons (Andrews and others, 2014; Ryser and others, 2014a, 2014b).

At the FOXX location, subglacial water pressures were measured in both boreholes and moulins. In 2011, seven boreholes were drilled using standard hot water drilling techniques (e.g. Andrews and others, 2014; Ryser and others, 2014a, 2014b). The three boreholes instrumented with pressure transducers had depths of 614–624 m and either did not drain or drained slowly following instrumentation. In 2011, one moulin, ~0.3 km from the borehole locations, was instrumented with a pressure transducer. In 2012, two additional moulins, that were located 1.6 and 1.9 km from the boreholes, were instrumented with pressure transducers. Details regarding instrumentation methodologies, instrument characteristics, duration, and the conversion of water level to hydraulic head can be found in Andrews and others (2014) and Ryser and others (2014a, 2014b).

In addition to subglacial measurements, Andrews and others (2014, 2018) derived both ice motion and bed separation from GPS positions at the FOXX and other locations. The station design was based on UNAVCO standards for polar regions and antenna height was independent of ice surface ablation (Andrews and others, 2014). At FOXX, GPS satellite information was recorded every 15 s using a Trimble Net R5 receiver and

Trimble Zephyr Geodetic antenna. Kinematic GPS positions were estimated using carrier-phase differential processing relative to a bedrock reference station using TRACK v1.24 (Chen, 1998) and final International GNSS Service satellite orbits. The 15-s time series was smoothed with a 450-minute moving-average window to remove erratic data (Fig. S4).

Bed separation calculations were performed using several surrounding GPS stations following procedures detailed in Hoffman and others (2011) and Andrews and others (2014, 2018). Vertical motion at the ice surface is the combination of the vertical component of mean bed-parallel motion, vertical strain and vertical motion of the basal ice relative to the bed (bed separation or cavity formation in the absence of sediments; Anderson and others, 2004; Hoffman and others, 2011). To isolate ice-bed separation (i.e. cavity opening) (Fig. S4), Andrews and others (2014) used common procedures to remove vertical strain in the ice column and bed-parallel motion from surface elevation measurements (e.g. Mair and others, 2001; Anderson and others, 2004; Howat and others, 2008; Hoffman and others, 2011). The components of vertical motion and their uncertainties are documented in Andrews and others (2014, 2018).

2.3 Rate and state framework

RSF is a phenomenological relationship that links friction of an interface to the rate of slip and state of the contacts between two surfaces. RSF has the capability to represent steady-state slip and describe aspects of transient slip. Such a framework has been applied to surging glaciers (Thøgersen and others, 2019; Minchew and Meyer, 2020) and seismogenic slip of soft-bedded glaciers (Lipovsky and Dunham, 2016, 2017). RSF has also been used to interpret glacial seismicity for hard-bedded slip (Zoet and others, 2013, 2020; Gräff and Walter, 2021) and to infer links between slip and subglacial cavity development (Thøgersen and others, 2019). RSF can be used to estimate the slip evolution from one sliding velocity to another through the incorporation of a 'direct effect', which characterizes the initial change in friction under a steady-state effective pressure, and the 'evolution effect', which characterizes the return to new steady-state friction (Fig. 3). Friction, μ, can be expressed as follows:

$$\mu \equiv \mu(V, \theta) = \mu_0 + a \ln\left(\frac{V}{V_0}\right) + b \ln\left(\frac{V_0\theta}{D_c}\right), \qquad (1)$$

where a parameterizes the magnitude of the direct effect, b parameterizes the magnitude of the drag evolution back to a new steady state, D_c is the critical slip distance where the friction decays $1/e$ from peak friction to the new steady-state, θ is the state variable that describes the state of ice-bed contact, V_0 is the initial velocity, V is the new velocity and μ_0 is reference
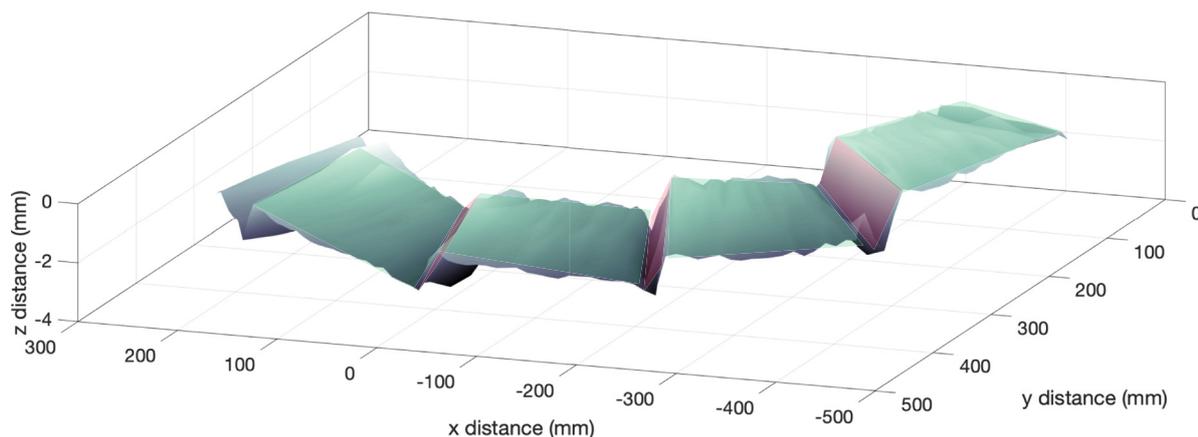
Fig. 4. Cavity geometry. Morphology of a portion (~1/4) of the ice sole measured at the final sliding speed (290 m a^{-1}). In this plot, the shaded green sections represent the cavity roofs, and the shaded pink sections represent the areas where the ice was in contact with the uppermost, up-glacier-facing parts of bumps on the bed like those shown in Figure 2.

friction at V_0 (Fig. 3). In effect, the value a-b represents the steady-state response of the system and relates to slip rules from process-based analyses (e.g. Weertman, double-valued, regularized Coulomb, etc.). The evolution in drag that occurs at the times (or displacements) between one steady state and the next, in response to a change in slip velocity, is not described in traditional steady-state slip laws and is the focus of this study.

The state variable, θ, in fault mechanics, is traditionally understood to represent the evolution of asperity contacts at a microscopic scale (Marone, 1998), but the phenomenological nature of RSF means that it can potentially be used to explain larger-scale processes such as cavity evolution (Thøgersen and others, 2019), provided an 'evolution law' can describe the evolution of cavity shape with time (or displacement). Such an evolution law, in conjunction with Eqn (1), can be used to estimate drag as a function of slip velocity and effective pressure in an evolving system. For cavity development, such an evolution law should describe the 'state' of the ice-bed contact through time in response to a velocity change, where θ could be physically thought of as the degree of ice-bed contact at some instant. We can use our experimental measurements of cavity-size evolution in response to velocity steps to determine an appropriate form for cavity evolution. We choose the following evolution law:

$$\dot{\theta} = 1 - \left(\frac{V\theta}{D_c}\right)^p, \quad (2)$$

where $\dot{\theta}$ is the time derivative of θ and p is an exponent related to ice flow. The form of Eqn (2) implies that the time evolution of θ depends on its current state and how far away cavity geometry is from the new steady configuration. Eqn (2) can represent the slip displacement needed for cavity geometry to evolve to a new steady state. The cavity evolution will happen quickly at first and then occur more slowly as the cavity approaches the new steady-state geometry. However, to use Eqns (1) and (2) to predict transient cavity and drag evolution, certain parameters need to be estimated, namely a, b and D_c. Their values are difficult to estimate from field data, where abrupt and then sustained velocity steps are rare. Therefore, we use our experimental data to measure how a, b and D_c vary in response to different velocity perturbations (Fig. 3 and Fig. S5).

2.4 Rate and state numerical estimates

With experimental values of a, b and D_c, Eqns (1) and (2) can be simultaneously solved to estimate time series of friction and state in response to velocity changes for a given apparatus stiffness $(0.6 \times 10^{-4} \, \mu\text{m}^{-1})$. To iteratively solve Eqns (1) and (2), we use

**Table 1.** Experimental results of velocity steps

V_0 (m a^{-1})	V (m a^{-1})	a (−)	b (−)	D_c (cm)
14.5	29	0.108	0.184	19.4
29	58	0.071	0.127	15.9
58	116	0.058	0.11	18.5
116	290	0.052	0.120	31.5

the *Rate and State Friction Toolkit* by Leeman and others (2016), which is a Python module that enables modeling of frictional response to dynamic events such as velocity steps and time-dependent frictional healing. This toolkit also provides the ability to apply a wide variety of evolution laws including Eqn (2), which can differ slightly from the more commonly used 'slowness' law developed for tectonic faults (Marone, 1998). First, we use this toolkit to generate a drag-and-state time series that is forced with the a, b and D_c variables measured from the experiments. The RSF toolkit-generated time series is then compared with the magnitude and timescale of drag evolution recorded in our experiments. We are thus able to compare the drag response estimated by the RSF model with the experimentally measured drag. We also qualitatively compare the state evolution from the RSF model with the cavity volume evolution measured in the experiments. As θ is a proxy for the state of ice-bed contact, the form of the state-evolution response should closely mimic the cavity-evolution response observed in the experiment if the form chosen for Eqn (2) is appropriate. Instances where the value of a-b is negative in response to a velocity increase, such that the new steady-state friction is reduced below its former value, are commonly referred to as velocity weakening, as opposed to velocity strengthening when the a-b value is positive (see Zoet and others, 2013, 2020; McCarthy and others, 2017; Saltiel and others, 2021).

Once the simple velocity steps from the experiment are simulated using the RSF Toolkit, a more dynamic case is simulated by forcing the RSF model's driving velocity with the constantly varying surface velocities measured from the Pâkitsoq region of the GIS (section 2.2). Driving the model with measured surface velocities generates a state-evolution response that can be compared with the field-data proxy for ice-bed separation (section 2.2). The model output allows the assessment of timing relationships among slip velocity, cavity size and basal drag.

3. Results and physical interpretations

In response to instantaneous velocity steps of experiments, the stress took anywhere from 3 to 12 d to return to a steady state, and in all cases, cavities coevolved with the stress (Fig. S5). The
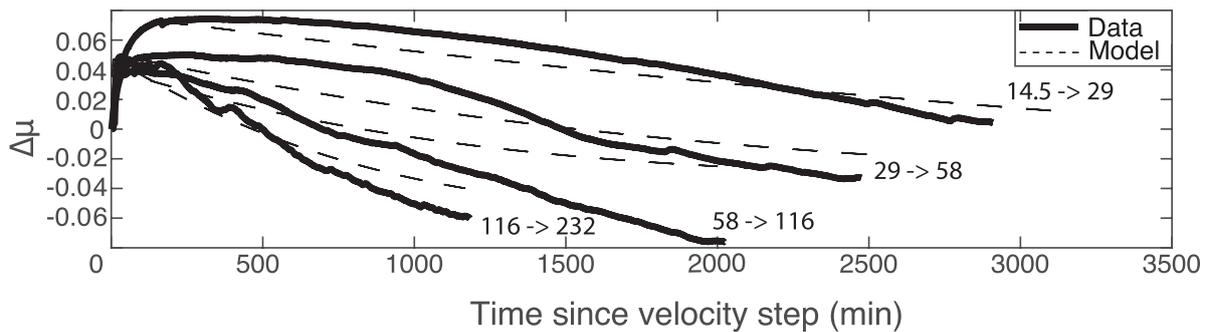
Fig. 5. Modeled experimental drag evolution. The solid black lines represent the experimental drag evolution in response to four near-instantaneous velocity steps, with their magnitudes indicated in m a⁻¹. The dashed lines are the RSF model predictions of the drag evolution using the parameters in Table 1 and Eqns (1) and (2). Initial drag values have been normalized to zero for comparison.

experimental timescales to achieve a steady state were longer (in some cases much longer) than the timescales on which velocity varied in the field data (Fig. S4). For each of the experimental velocity steps, a, b and D_c were measured (Table 1). All velocity steps first resulted in an initial increase in stress that then decayed to a new steady-state value after some displacement (Fig. 3 and Fig. S5). For this experiment, the steady-state drag values at the new higher velocity were less than those of the previous lower velocity, which was expected for the sinusoidal bed of the experiment (Schoof, 2005; Gagliardini and others, 2007; Zoet and Iverson, 2015), but the initial stress increase illustrates that temporary strengthening can occur even with a rate-weakening slip law (Fig. 1).

Using the RSF parameter values estimated from the velocity-stepping experiments (Table 1), drag evolution after velocity steps was modeled (Fig. 5). The p value was set to equal 1 (see Fig. S6 for other choices of p). Findings by Adams and others (2021) show the exponent on the ice flow law for temperate ice with sufficient intercrystalline water is equal to 1.1, which may in part indicate why $p = 1$ was found to best approximate the cavity evolution response in the experiments. The RSF model describes the timescale and magnitude of the drag change well but does not precisely replicate its form. The mismatch in the drag evolution likely stems from the generalized form of Eqn (2), which explicitly contains no information about obstacle size. Nevertheless, Eqn (2) does qualitatively match the time and length scale of the observed cavity change (Fig. 6).

Using the parameters measured from the experiment (Table 1), we select RSF parameter values from one velocity step to model the continuously evolving slip of the GIS with the RSF Toolkit, as forced by GIS surface velocity measurements and drag estimates from the field. Specifically, the RSF parameters measured from the experimental velocity step from 116 to 290 m a⁻¹ (Table 1) are used in the GIS modeling because they most closely represent the range of velocities observed at FOXX (80–180 m a⁻¹, Fig. S4), but a range of other a, b and D_c values were also modeled to examine their effect on the transient drag response (Fig. S7). The model was forced with a 10-day time series extracted from the 2012 FOXX dataset for days 195–205. Figure 7a compares the modeled state variable (note the scale has been flipped for comparison with Fig. 7b) – a proxy for cavity size – with the driving velocity. Maximum state values lag the velocity maximums by a mean of 4.0 h. Figure 7b shows a comparison of the velocity and the field-derived ice-bed separation. Maximum field ice-bed separation values lag the velocity maximums by a mean of 4.7 h. The difference between the modeled and observed lags (∼0.7 h) is small in comparison to the magnitudes of the observed lags (∼15%). This agreement between the model results and data indicates that the model adequately describes the lag period for cavity development. This lag reflects

the time required for cavities in the natural system to respond to velocity changes. Additionally, Hoffman and others (2018) used an ice flow model constrained by GPS-derived ice velocities to invert for basal traction in the Påkitsoq region in response to diurnal melt forcing prior to a glacial lake drainage event. They found that basal shear traction varied by 15% in response to diurnal variations in meltwater delivery to the bed. Using the RSF model (Fig. 8a) forced by the diurnal velocity signal at the same general location we find that friction varies by ±18% from the steady state value $\mu_0 = 0.17$, where μ_0 was estimated from the steady-state drag of the initial velocity (see supporting text S2 for a detailed explanation of the double-valued steady-state sliding response). Our modeled variation of basal traction is in seemingly good agreement with the inversion findings of Hoffman and others (2018). It is noteworthy that none of the RSF model predictions has been tuned to fit results from this location. Rather the RSF model is independently derived from the results of the laboratory experiments. This agreement between the field observations and laboratory-based model results, despite likely differences between the scales of experimental and natural bed obstacles, provides some degree of confidence that the empirical model includes aspects of the physics that regulate the transient slip response. Thus, investigating the modeled relationships among slip velocity, cavity size and drag may provide insights into basal processes.

In comparing the velocity time series with the state and drag responses, lags are apparent that can be used to infer physical processes. Figure 8 shows that the peak in drag often occurs when sliding velocity is high (but not at its maximum), and cavities are small. This is well represented in Figure 8a for days 198–203. A simple explanation for this pattern is that, as velocity increases, cavities are initially small and must grow to reach the new steady-state size. The associated initial excess in the ice-bed contact area together with a high slip velocity requires more force and hence shear stress to drag ice past bed obstacles. As the cavities grow and ice-bed contact areas become smaller the drag begins to decrease. The maximum in drag, while velocity is increasing, arises because cavity size is sufficiently close to the new steady-state value that further growth reduces the drag. In part, the drag response also stems from the direct effect causing the initial proportional change in resistance in response to a velocity change. Given the ever-changing velocity of the natural system, the direct effect's response could dominate in certain instances (see Fig. S7).

To illustrate the limitations of applying a steady-state sliding rule, we now compare the transient drag response based on the RSF model with drag calculated from the steady-state, double-valued sliding law (Zoet and Iverson, 2015) that reflects the measured a-b values. This sliding relation agreed with experimental observations and was derived from the cavity model of Kamb
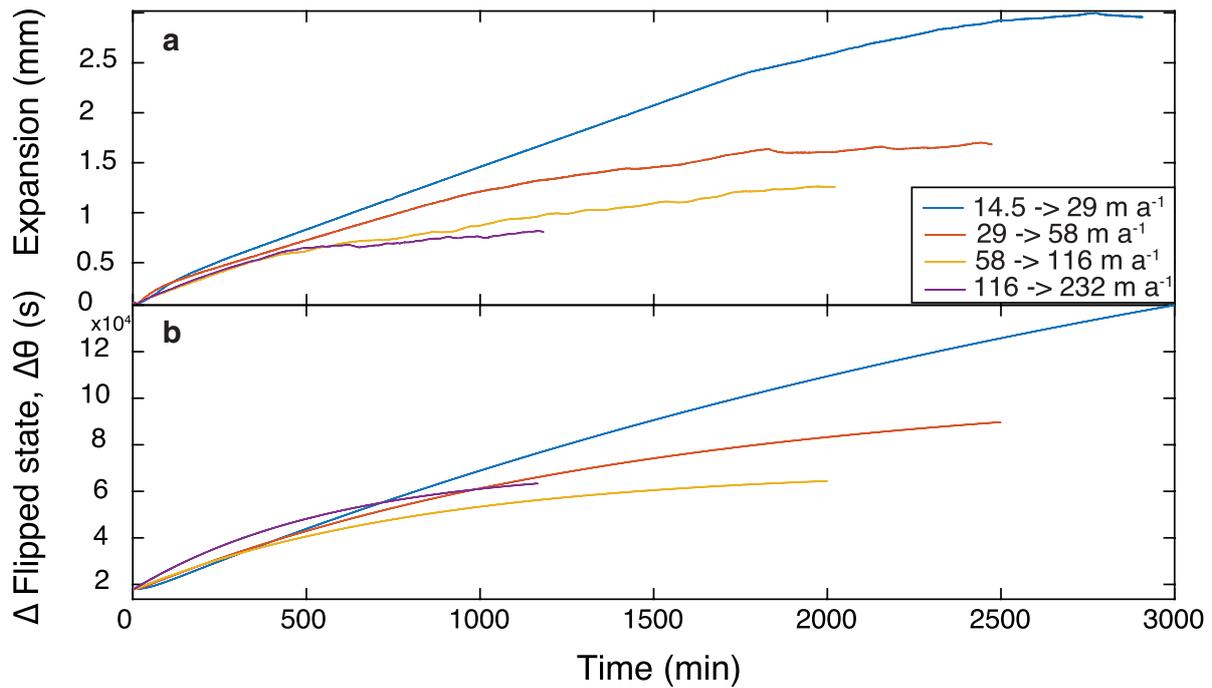
Fig. 6. Cavity and state evolution. (a) Cavity evolution was recorded by the increases in thickness of the ice chamber in response to four near-instantaneous velocity steps. Positive displacements indicate expansion of the ice chamber from cavity growth. The background melt rate was estimated prior to the slip and removed from the signal leaving mainly cavity expansion and contraction. (b) State evolution predicted by the RSF model using Eqn (2) with $p = 1$ and the parameters in Table 1. Initial state values have been offset to 0 (hence $\Delta\theta$) and then flipped for ease of comparison with the cavity expansion record. The measured displacement and predicted state evolution are similar indicating Eqn (2) adequately describes cavity evolution.
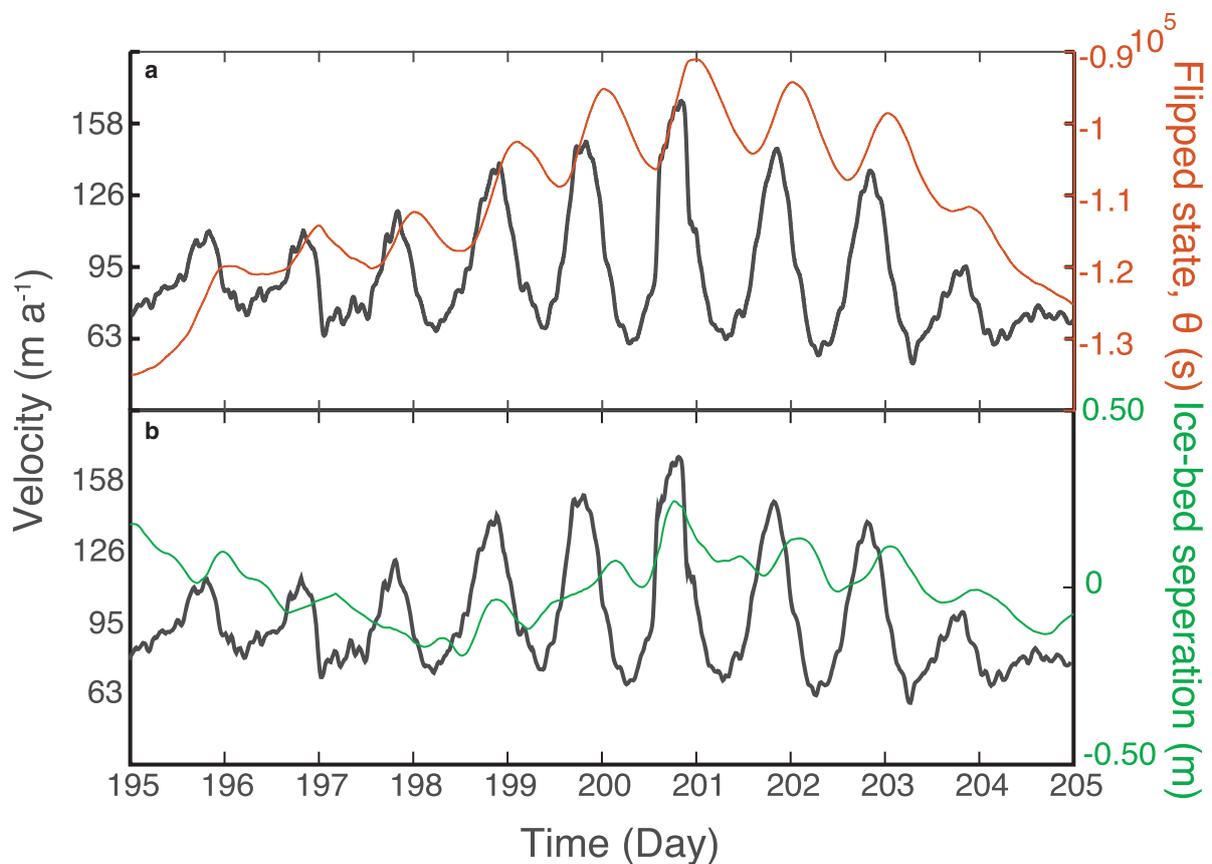
Fig. 7. Modeled and observed glacier cavity evolution. The solid black line is the surface velocity, recorded for 10 d in 2012 at the GIS FOXX site, which is used to drive the RSF model. (a) The state and velocity time series. The state variable has been flipped for comparison (multiplied by −1), so values closer to zero (up on the plot) represent larger cavities. The state variable, which is a proxy for cavity development, lags the velocity because of the time required for cavities to adjust to changes in velocity. (b) The observed field proxy for ice-bed separation was estimated by Andrews and others (2014) for the FOXX site. The field proxy for ice-bed separation also lags velocity. Both the observed and modeled ice-bed separation lag velocity by ∼4 h, indicating the RSF model reasonably replicates the timescale of cavity development that is indicated by the field data.
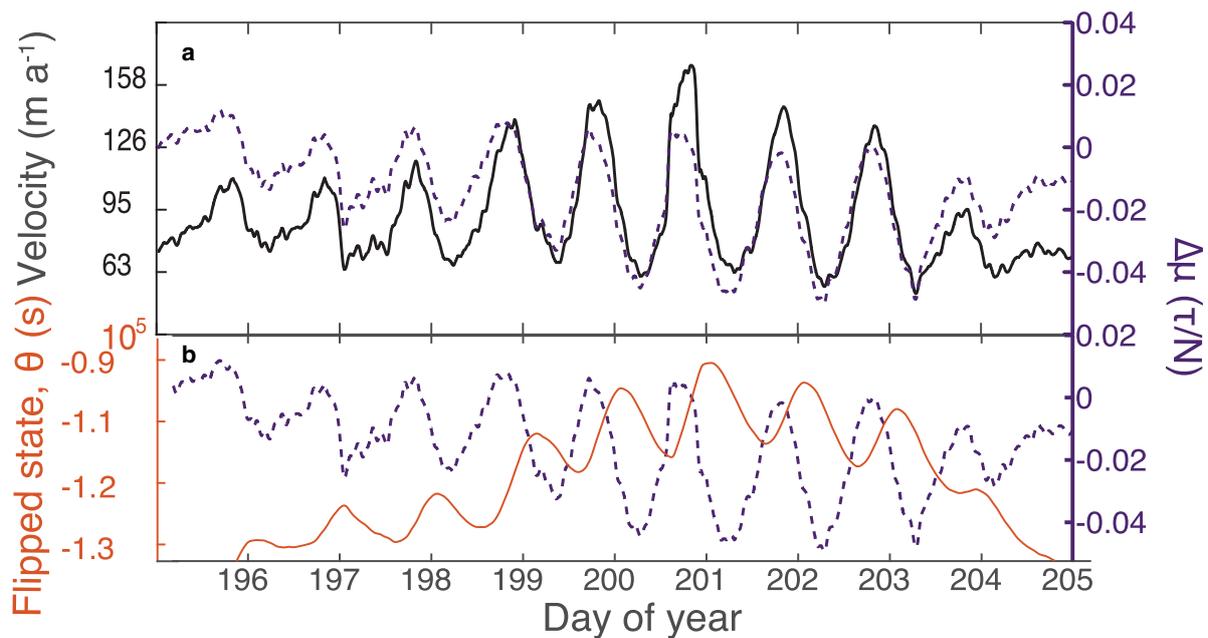
Fig. 8. Model drag response. (a) GIS velocity was used to drive the model (black line) compared with the drag response (purple dashed line). Drag peaks prior to maximum velocity in many instances (e.g. days 198–203) (b) RSF-estimated drag (purple dashed line) compared with the state value (cavity proxy). Drag peaks when the cavity geometry (flipped state value) is small. As the cavity grows, the drag begins to decrease. Note drag has been shifted to zero, so only changes are shown.

(1987) and the sliding model of Lliboutry (1968, 1979) (see supporting text S2 for more details). To normalize the drag in the RSF model, we divide the shear stress by $N = 40$ kPa, which was approximately the value measured by Andrews and others (2014) for the FOXX site. Figure 9 shows the comparison of the normalized drag (i.e. the friction, $\mu = \tau/N$) for the steady state and transient models. Importantly, the drag in the two cases is nearly fully out of phase. The large disagreement between peak-drag phasing of these two models illustrates the effect of transient cavity adjustment on drag.

4. Discussion

Our results indicate that the transient drag response controls the timing of drag fluctuations at this GIS location. There is good agreement between the phasing of the measured ice-bed separation and that predicted by the RSF model with its parameters based on experimental values (Fig. 7). Importantly, a substantial lag exists between peak drag based on the steady-state double-valued sliding law and that based on the RSF model (Fig. 9). The differences in the timing of the drag result from the steady-state model's absence of processes associated with cavity growth or shrinkage. Furthermore, the transient increase in drag associated with a velocity change can be larger than the change in steady-state stress (i.e. $|a| > |a - b|$), highlighting that the transient response should have a major effect on the drag for some of the duration of cavity adjustment during slip. In these instances, the glacier would in effect need to overcome this temporary local increase in slip resistance (in the case of a velocity increase) to reach the new steady state. This would be possible if the section of the bed producing the transient strengthening is small in area or the strengthening is small in magnitude. However, if the area or magnitude is sufficiently large, it may not be possible for the glacier to develop longitudinal or transverse stress gradients sufficient to increase the local slip velocity.

Cavity sizes at the base of the GIS and those of our laboratory experiments are likely quite different. Therefore, it is surprising that the RSF model results, as parameterized by our small-scale

experiments, match the observed field data well, especially considering that no model tuning was performed. This agreement seems to suggest that scale-normalized processes are active that allow the lab findings to scale up to the field setting. For example, although D_c might be expected to be larger in the field than in the experiments, the closure rates of cavities may increase nonlinearly with increasing cavity size, leading to shorter response times. One source of such nonlinearity could arise from a decrease in water pressure within cavities as they open, owing to the increased cross-sectional area for water flow, causing increments of cavity growth to be accompanied by increments of increasing effective pressure (see Bartholomaus and others, 2011; Hoffman and Price, 2014). Another potential source of closure rates increasing nonlinearly with cavity size stems from the nonisolated nature of cavities when there is pervasive ice-bed separation (Helanow and others, 2021; Mejía and others, 2021), unlike the isolated boreholes (Nye, 1953) or cracks that are used as the basis for estimating cavity closure rates (Walder, 1986; Kamb, 1987). As cavities grow, intervening zones of ice become increasingly narrow so that deviatoric stresses in the ice cause closure rates to increase more rapidly than if cavities are isolated (Zoet and Iverson, 2016).

Given the paucity of field data and the nonunique nature of its response to a myriad of physical processes, it is impossible to directly determine the exact combination of physical processes that are driving glacier dynamics at any one location. A systematic approach that includes using experimentation to constrain some of the fundamental physical processes and associated parameters provides a useful tool for interpreting field data, but we acknowledge the ambiguity in linking field data to simplified scenarios like those proposed here. With the limited experimental data and a relatively small number of field observations of cavity size, we cannot fully explore the effects of the cavity scale without more observations. More experimental work is needed to better constrain how the parameters a, b and perhaps most importantly D_c vary under different bed conditions and effective pressures.

This RSF analysis could provide a method to interpret links among velocity, drag and water pressure directly from measurements on glaciers, where interpretations traditionally are limited
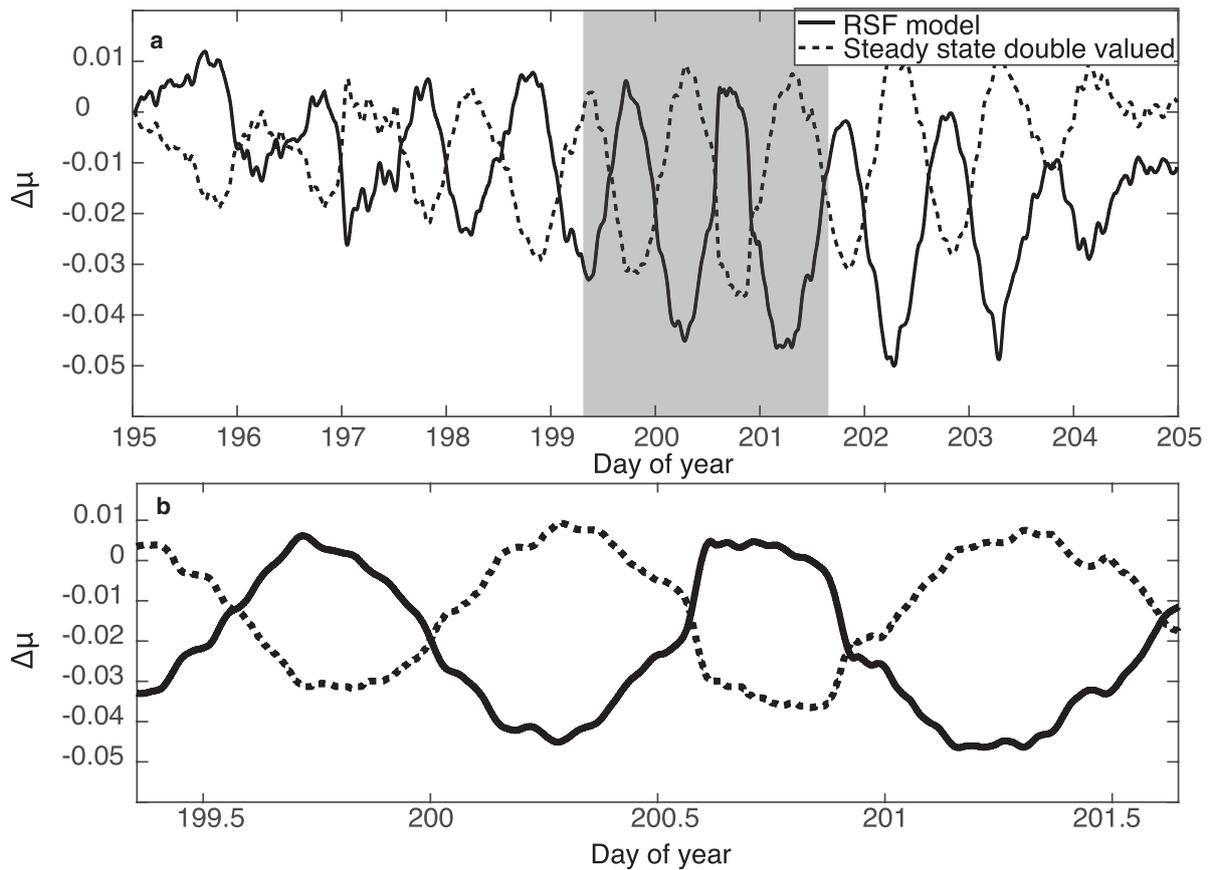
Fig. 9. Steady-state vs. transient drag. (a) Drag estimated from a steady-state, double-valued model (dashed black line) compared with that of the RSF model (solid black line). (b) Detail of ~2 d (grey bar in the upper panel). The timing offset between these two results stems from transient effects not included in the steady-state approximation.

by competing effects that are difficult to isolate. The nature of the *a-b* values in this study (Table 1) means that the steady-state response is that of a rate-weakening slip law (Zoet and Iverson, 2015), but importantly this type of transient RSF analysis could be applied with any steady-state slip law (e.g. regularized Coulomb or Weertman) by adjusting the *a-b* values in the RSF model. This RSF model does not supplant steady-state slip laws, but in the presence of sufficiently high-frequency fluctuations in velocity or water pressure, descriptions of slip dynamics would benefit from the transient RSF model being applied alongside estimates from steady-state slip laws.

5. Conclusions

Transient slip behavior measured in experiments and applied to the time series from the GIS indicate that transient slip processes control drag in regions of rapidly changing basal conditions. The experimental results are reasonably well approximated by a RSF model that describes transient slip. The experimentally calibrated RSF model driven by surface-velocity time series from the GIS yields lags in cavity development with respect to surface velocity like those observed in the field. As velocity increases, drag is initially large because cavities are small and transiently large contact areas at the higher sliding velocity require greater forces and hence shear stress to drive ice flow past obstacles on the bed. Shear stress decreases as cavities grow and ice-bed contact decreases. The peaks in drag indicated by the steady-state and RSF models are almost completely out of phase, demonstrating the importance of considering transient effects on drag. The steady-state model applied here is based on the rate-weakening part of the double-valued sliding law, but the RSF model can be

applied to any steady-state sliding law by adjusting the *a* and *b* parameters. The transient response will likely be important at locations where basal conditions are changing faster than the timescale for growth or shrinkage of cavities at the bed. In such locations, transient stresses associated with cavity volume change can control basal drag and thus should be incorporated in models of glacier flow.

References

Adams C, Iverson NR, Helanow C, Zoet LK and Bate CE (2021) Softening of temperate ice by interstitial water. *Frontiers in Earth Science* **9**, 590. doi: 10.3389/feart.2021.702761

Anderson RS and 6 others (2004) Strong feedbacks between hydrology and sliding of a small Alpine glacier. *Journal of Geophysical Research: Earth Surface* **109**(F3), F03005. doi: 10.1029/2004JF000120

Andrews LC and 5 others (2014) Direct observations of evolving subglacial drainage beneath the Greenland ice sheet. *Nature* **514**(7520), 80–83. doi: 10.1038/nature13796

Andrews LC and 5 others (2018) Seasonal evolution of the subglacial hydrologic system modified by supraglacial lake drainage in Western Greenland.

Journal of Geophysical Research: Earth Surface **123**(6), 1479–1496. doi: [10.1029/2017JF004585](10.1029/2017JF004585)

Bartholomaus TC, Anderson RS and Anderson SP (2008) Response of glacier basal motion to transient water storage. *Nature Geoscience* **1**(1), 33–37. doi: 10.1038/ngeo.2007.52

Bartholomaus TC, Anderson RS and Anderson SP (2011) Growth and collapse of the distributed subglacial hydrologic system of Kennicott glacier, Alaska, USA, and its effects on basal motion. *Journal of Glaciology* **57** (206), 985–1002. doi: [10.3189/002214311798843269](10.3189/002214311798843269)

Bindschadler R (1983) The importance of pressurized subglacial water in separation and sliding at the glacier bed. *Journal of Glaciology* **29**(101), 3–19. doi: [10.3189/S0022143000005104](10.3189/S0022143000005104)

Chen G (1998) *GPS kinematic Positioning for Airborne laser Altimetry at Long Valley, California*. Cambridge, MA: Massachusetts Institute of Technology. Retrieved from http://dspace.mit.edu/handle/1721.1/9680.

Covington MD, Gulley JD, Trunz C, Mejia J and Gadd W (2020) Moulin volumes regulate subglacial water pressure on the Greenland ice sheet. *Geophysical Research Letters* **47**(20), e2020GL088901. doi: [10.1029/2020GL088901](10.1029/2020GL088901)

Cowton T and 5 others (2013) Evolution of drainage system morphology at a land-terminating Greenlandic outlet glacier. *Journal of Geophysical Research: Earth Surface* **118**(1), 29–41. doi: [10.1029/2012JF002540](10.1029/2012JF002540)

Fischer UH and Clarke GK (1997) Stick–slip sliding behaviour at the base of a glacier. *Annals of Glaciology* **24**, 390–396. doi: [10.3189/S0260305500012490](10.3189/S0260305500012490)

Flowers GE (2015) Modelling water flow under glaciers and ice sheets. *Proceedings of the Royal Society A: Mathematical, Physical and Engineering Sciences* **471**(2176), 1–47. doi: 10.1098/rspa.2014.0907.

Gagliardini O, Cohen D, Råback P and Zwinger T (2007) Finite-element modeling of subglacial cavities and related friction law. *Journal of Geophysical Research: Earth Surface* **112**(F2), F02027. doi: [10.1029/2006JF000576](10.1029/2006JF000576)

Gräff D and Walter F (2021) Changing friction at the base of an Alpine glacier. *Scientific Reports* **11**(1), 1–10. doi: [10.1038/s41598-021-90176-9](10.1038/s41598-021-90176-9)

Harper JT, Humphrey NF and Greenwood MC (2002) Basal conditions and glacier motion during the winter/spring transition, Worthington glacier, Alaska, USA. *Journal of Glaciology* **48**(160), 42–50. doi: [10.3189/172756502781831629](10.3189/172756502781831629)

Harper JT, Humphrey NF, Pfeffer WT and Lazar B (2007) Two modes of accelerated glacier sliding related to water. *Geophysical Research Letters* **34** (12), L12503. doi: [10.1029/2007GL030233](10.1029/2007GL030233)

Helanow C, Iverson NR, Woodard J and Zoet LK (2021) A slip law for hard-bedded glaciers derived from observed bed topography. *Science Advances* **7**(20), eabe7798. doi: 10.1126/sciadv.abe7798

Helanow C, Iverson NR, Zoet LK and Gagliardini O (2020) Sliding relations for glacier slip with cavities over three-dimensional beds. *Geophysical Research Letters* **47**(3), e2019GL084924. doi: [10.1029/2019GL084924](10.1029/2019GL084924)

Hewitt IJ (2011) Modelling distributed and channelized subglacial drainage: the spacing of channels. *Journal of Glaciology* **57**(202), 302–314. doi: [10.3189/002214311796405951](10.3189/002214311796405951)

Hoffman MJ and 6 others (2018) Widespread moulin formation during supraglacial lake drainages in Greenland. *Geophysical Research Letters* **45** (2), 778–788. doi: [10.1002/2017GL075659](10.1002/2017GL075659)

Hoffman MJ, Catania GA, Neumann TA, Andrews LC and Rumrill JA (2011) Links between acceleration, melting, and supraglacial lake drainage of the western Greenland ice sheet. *Journal of Geophysical Research: Earth Surface* **116**(F4), F04035. doi: [10.1029/2010JF001934](10.1029/2010JF001934)

Hoffman MJ and Price S (2014) Feedbacks between coupled subglacial hydrology and glacier dynamics. *Journal of Geophysical Research: Earth Surface* **119**(3), 414–436. doi: [10.1002/2013JF002943](10.1002/2013JF002943)

Hooke RL, Hanson B, Iverson NR, Jansson P and Fischer UH (1997) Rheology of till beneath Storglaciären, Sweden. *Journal of Glaciology* **43** (143), 172–179. doi: [10.3189/S0022143000002938](10.3189/S0022143000002938)

Howat IM, Tulaczyk S, Waddington E and Björnsson H (2008) Dynamic controls on glacier basal motion inferred from surface ice motion. *Journal of Geophysical Research: Earth Surface* **113**(F3), F03015. doi: [10.1029/2007JF000925](10.1029/2007JF000925)

Iken A (1972) Measurements of water pressure in moulins as part of a movement study of the White glacier, Axel Heiberg Island, Northwest Territories, Canada. *Journal of Glaciology* **11**(61), 53–58. doi: [10.3189/S0022143000022486](10.3189/S0022143000022486)

Iken A (1981) The effect of the subglacial water pressure on the sliding velocity of a glacier in an idealized numerical model. *Journal of Glaciology* **27**(97), 407–421. doi: [10.3198/1981JoG27-97-407-421](10.3198/1981JoG27-97-407-421)

Iken A and Bindschadler RA (1986) Combined measurements of subglacial water pressure and surface velocity of Findelengletscher, Switzerland:

conclusions about drainage system and sliding mechanism. *Journal of Glaciology* **32**(110), 101–119. doi: [10.3189/S0022143000006936](10.3189/S0022143000006936)

Iverson NR and Petersen BB (2011) A new laboratory device for study of subglacial processes: first results on ice–bed separation during sliding. *Journal of Glaciology* **57**(206), 1135–1146. doi: [10.3189/002214311798843458](10.3189/002214311798843458)

Kamb B and others (1985) Glacier surge mechanism: 1982-1983 surge of Variegated glacier, Alaska. *Science (New York, N.Y.)* **227**(4686), 469–479. doi: 10.1126/science.227.4686.469

Kamb B (1987) Glacier surge mechanism based on linked cavity configuration of the basal water conduit system. *Journal of Geophysical Research: Solid Earth* **92**(B9), 9083–9100. doi: [10.1029/JB092iB09p09083](10.1029/JB092iB09p09083)

Leeman JR, May R, Marone C and Saffer D (2016) *Modeling Rate-and-State Friction with Python*. GitHub: SciPy Scientific Programming.

Lipovsky BP and Dunham EM (2016) Tremor during ice-stream stick slip. *The Cryosphere* **10**(1), 385–399. doi: [10.5194/tc-10-385-2016](10.5194/tc-10-385-2016)

Lipovsky BP and Dunham EM (2017) Slow-slip events on the Whillans ice plain, Antarctica, described using rate-and-state friction as an ice stream sliding law. *Journal of Geophysical Research: Earth Surface* **122**(4), 973–1003. doi: [10.1002/2016JF004183](10.1002/2016JF004183)

Lliboutry L (1968) General theory of subglacial cavitation and sliding of temperate glaciers. *Journal of Glaciology* **7**(49), 21–58. doi: [10.3189/S0022143000020396](10.3189/S0022143000020396)

Lliboutry L (1979) Local friction laws for glaciers: a critical review and new openings. *Journal of Glaciology* **23**(89), 67–95. doi: [10.3189/S0022143000029750](10.3189/S0022143000029750)

Mair D, Nienow P, Willis I and Sharp M (2001) Spatial patterns of glacier motion during a high-velocity event: Haut glacier d'Arolla, Switzerland. *Journal of Glaciology* **47**(156), 9–20. doi: [10.3189/172756501781832412](10.3189/172756501781832412)

Marone C (1998) Laboratory-derived friction laws and their application to seismic faulting. *Annual Review of Earth and Planetary Sciences* **26**(1), 643–696. doi: 10.1146/annurev.earth.26.1.643

McCarthy C, Savage H and Nettles M (2017) Temperature dependence of ice-on-rock friction at realistic glacier conditions. *Philosophical Transactions of the Royal Society A: Mathematical, Physical and Engineering Sciences* **375**(2086), 20150348. doi: 10.1098/rsta.2015.0348

Mejía JZ and 6 others (2021) Isolated cavities dominate Greenland ice sheet dynamic response to lake drainage. *Geophysical Research Letters* **48**, e2021GL094762. doi: [10.1029/2021GL094762](10.1029/2021GL094762)

Minchew BM and Meyer CR (2020) Dilation of subglacial sediment governs incipient surge motion in glaciers with deformable beds. *Proceedings of the Royal Society A* **476**(2238), 20200033. doi: 10.1098/rspa.2020.0033

Nye JF (1953) The flow law of ice from measurements in glacier tunnels, laboratory experiments and the Jungfraufirn borehole experiment. *Proceedings of the Royal Society of London. Series A. Mathematical and Physical Sciences* **219**(1139), 477–489. doi: 10.1098/rspa.1953.0161

Ryser C and 5 others (2014a) Caterpillar-like ice motion in the ablation zone of the Greenland ice sheet. *Journal of Geophysical Research: Earth Surface* **119**(10), 2258–2271. doi: [10.1002/2013JF003067](10.1002/2013JF003067)

Ryser C and 5 others (2014b) Sustained high basal motion of the Greenland ice sheet revealed by borehole deformation. *Journal of Glaciology* **60**(222), 647–660. doi: [10.3189/2014JoG13J196](10.3189/2014JoG13J196)

Saltiel S, McCarthy C, Creyts TT and Savage HM (2021) Experimental evidence of velocity-weakening friction during ice slip over frozen till: implications for basal seismicity in fast moving, soft-bed glaciers and ice streams. *Seismological Research Letters*, 2793–2810. doi: [10.1785/0220200480](10.1785/0220200480).

Schoof C (2005) The effect of cavitation on glacier sliding. *Proceedings of the Royal Society A: Mathematical, Physical and Engineering Sciences* **461** (2055), 609–627. doi: 10.1098/rspa.2004.1350

Thøgersen K, Gilbert A, Schuler TV and Malthe-Sørenssen A (2019) Rate-and-state friction explains glacier surge propagation. *Nature Communications* **10**(1), 1–8. doi: [10.1038/s41467-019-10506-4](10.1038/s41467-019-10506-4)

Tsai VC, Smith LC, Gardner AS and Seroussi H (2021) A unified model for transient subglacial water pressure and basal sliding. *Journal of Glaciology* **67**, 1–11. doi: [10.1017/jog.2021.103](10.1017/jog.2021.103)

Walder JS (1986) Hydraulics of subglacial cavities. *Journal of Glaciology* **32**(112), 439–445. doi: [10.3189/S0022143000012156](10.3189/S0022143000012156)

Werder MA, Hewitt IJ, Schoof CG and Flowers GE (2013) Modeling channelized and distributed subglacial drainage in two dimensions. *Journal of Geophysical Research: Earth Surface* **118**(4), 2140–2158. doi: 10.1002/jgrf.20146

Zoet LK and 6 others (2013) The effects of entrained debris on the basal sliding stability of a glacier. *Journal of Geophysical Research: Earth Surface* **118** (2), 656–666. doi: doi.org/10.1002/jgrf.20052

Zoet LK and 6 others (2020) Application of constitutive friction laws to glacier seismicity. *Geophysical Research Letters* **47**(21), e2020GL088964. doi: 10.1029/2020GL088964

Zoet LK and Iverson NR (2015) Experimental determination of a double-valued drag relationship for glacier sliding. *Journal of Glaciology* **61**(225), 1–7. doi: 10.3189/2015JoG14J174

Zoet LK and Iverson NR (2016) Rate-weakening drag during glacier sliding. *Journal of Geophysical Research: Earth Surface* **121**(7), 1206–1217. doi: 10.1002/2016JF003909

Zoet LK and Iverson NR (2020) A slip law for glaciers on deformable beds. *Science (New York, N.Y.)* **368**(6486), 76–78. doi: 10.1126/science.aaz1183